

Article

Predicting Seismic Collapse Safety of Post-Fire Steel Moment Frames

Esmaeil Mohammadi Dehcheshmeh ¹, Parya Rashed ¹, Vahid Broujerdian ^{1,*}, Ayoub Shakouri ¹
and Farhad Aslani ^{2,*}

¹ School of Civil Engineering, Iran University of Science and Technology, Tehran 16846-13114, Iran; esmhd.dehcheshmeh@gmail.com (E.M.D.); p_rashed@alumni.iust.ac.ir (P.R.); m_shakoori@alumni.iust.ac.ir (A.S.)

² Materials and Structures Innovation Group, School of Engineering, University of Western Australia, Perth, WA 6009, Australia

* Correspondence: broujerdian@iust.ac.ir (V.B.); farhad.aslani@uwa.edu.au (F.A.)

Abstract: This paper summarizes a study focused on evaluating the post-fire performance of steel Intermediate Moment Frames (IMFs) following earthquakes. To this aim, archetypes comprising 3-bay IMFs with three different heights were seismically designed, and their two-dimensional finite element models were created in OpenSees software. The post-fire mechanical properties of steel were inserted into the models based on 64 different fire scenarios. The effects of different cooling methods are scrutinized at system level. To develop seismic fragility curves, Incremental Dynamic Analysis (IDA) was performed using 50 suites of far-field and near-field records, according to FEMA-P695. Then, the Collapse Margin Ratio (CMR) of each model was calculated based on the data from the fragility analysis. The results show that the seismic resistance of structures that experienced fire declines to some extent. In addition, the lowest safety level was observed when the structures were subjected to pulse-like near-field records.

Keywords: post-fire earthquake; intermediate moment frame; fire scenario; fragility curves; collapse margin ratio



Citation: Dehcheshmeh, E.M.; Rashed, P.; Broujerdian, V.; Shakouri, A.; Aslani, F. Predicting Seismic Collapse Safety of Post-Fire Steel Moment Frames. *Buildings* **2023**, *13*, 1091. <https://doi.org/10.3390/buildings13041091>

Academic Editors: Xavier Romão and Hugo Rodrigues

Received: 20 March 2023

Revised: 5 April 2023

Accepted: 18 April 2023

Published: 20 April 2023



Copyright: © 2023 by the authors. Licensee MDPI, Basel, Switzerland. This article is an open access article distributed under the terms and conditions of the Creative Commons Attribution (CC BY) license (<https://creativecommons.org/licenses/by/4.0/>).

1. Introduction

Steel structures are inherently prone to fire incidents. Although structural steel is noncombustible, its strength and stiffness can be compromised at high temperatures, followed by permanent large deformations. In most cases, the post-fire condition alone may not lead the structure to collapse, but problems arise when the structure sustains seismic loading after experiencing fire. Therefore, it is essential to gain comprehensive knowledge on the seismic performance level (PL) of steel structures after the fire incident which results in the degradation of material properties. Of course, whether a fire-exposed structure can be reliably reused or not is important in the first place [1].

The structural safety of steel structures in case of extreme circumstances such as fire is often addressed by many codes in qualitative, yet ambiguous ways. Therefore, structural engineers cannot achieve structural integrity by referring to specific code-based methodologies [2]. The integrity of steel structures in a post-fire condition is mainly influenced by the degradation of the steel material properties. Previous studies suggest that although the mechanical properties of steel decrease at elevated temperatures, the structure can completely or partially regain its initial properties after cooling down and returning to ambient temperature [3–8]. However, there are some major factors that affect this recovery process, namely the method of cooling down the metal and its rate, the maximum temperature of steel, the chemical composition of the metal, etc. [9]. When the steel members are rapidly cooled down from an elevated temperature in water or oil, the material hardens due to the formation of martensite, a very hard phase of steel. However,

when the cooling process is slower, then softer phases of metal will eventually form. If the same steel is cooled down in air or sand, it results in a softer material without the hard martensitic phase [10].

From a more general perspective, permanent deformations of structural components and their residual stresses after a fire event determine the chance of building reutilization [11–13]. Based on the literature, vulnerability functions on post-fire steel frames have been studied regarding which three types of damage degree can be defined for steel members: (1) structural components that appear to be straight or marginally distorted by around four times ASTM A6 rolling tolerances [14], a case in which no repair is needed; (2) members that sustain considerable deformation but could undergo heat-straightening, and which are replaced if possible; and (3) members that are so severely deformed that repair would be economically unfeasible compared to the cost of replacement due to the metallurgical changes affecting their load-bearing capacity. According to the experimental fire performance test data, it is anticipated that the last group is exposed to temperatures beyond 600 °C [15]. The extent of structural damage determines the reparability and reuse of the building. Furthermore, Weld et al. [16] demonstrated that the extent of damage to the members is not only affected by peak temperature, but also depends on the duration of fire exposure. Another major parameter affecting the post-fire state of steel components is the difference between cooling methods, some of which lead to lower fatigue strength [17].

The behavior of structures subjected to abnormal loadings such as fire is escalated following an earthquake event. The major problem arises from the heterogeneity of steel members after cooling down, material degradation, and residual deformations [15,18]. A study by Quayyum and Hassan [15] dealt with the seismic behavior of post-fire steel buildings whose fire originated from an earthquake event. Thermal analysis was carried out to develop a contour of temperature history throughout the steel components, and the results were used in thermomechanical analysis to examine their level of damage degree. Results showed that steel frames designed with heavy member sections like steel wide flange beams are prone to seismic vibrations in the case of not being repaired after fire. Moreover, the stories in which fire has been ignited have demonstrated a weak column-strong beam mechanism followed by soft-story failure due to plastic hinge formation in columns. Pantousa et al. [18] narrowed down the scale of study to steel columns with axial and rotational springs at the top ends serving as a boundary condition. Thermomechanical analysis was conducted as an initial condition for cyclic loading. The findings without considering boundary conditions indicated that at peak temperatures of less than or equal to 550 °C, local displacements of 1 mm resulted, which showed there to be no impact on the column behavior under cyclic loading. With the increase in maximum temperature, early mechanisms of local buckling generated near the footing, followed by a great reduction in the flexural capacity of columns. Three failure modes were observed: formation of plastic hinge, local buckling mechanism, and global instability of columns about the weak axis when demand does not exceed plastic moment capacity of the cross-section. However, lateral buckling only caused failure to columns with considerable damage. Regarding boundary conditions, studies have observed a reduction in the flexural and rotational capacity of columns during cyclic loading. Premature local buckling at the top end was found to be a failure mode induced by flexural deterioration.

Wang et al. [19] investigated the post-fire seismic performance of composite frames. The tests revealed that debonding along interfaces of steel and concrete is the major hazard in post-fire structures serving cyclic loading demands. Additionally, the ductility coefficient and the ultimate displacement of heated frames were shown to be larger than that of initial specimens subjected to cyclic loadings only. As for heating time, little effect was found on the frame stiffness and damping coefficient. In another study [17], the influences of elevated temperature on moment frame steel connections were fully experimented, and finite element models were developed with a close similarity to experimental practice.

More recently, researchers have assessed the seismic damage of steel moment-resisting frames by means of fragility curves, considering pounding effects [20], near-field ground

motions with high frequency content [21], and impact actions [22]. Use of fragility curves is also encouraged in post-fire seismic assessment of RC frames with elastomeric bearings [23].

The seismic behavior of fire-exposed steel structures has been addressed in few recent studies. Several approaches for damage detection and for preventing structures from early collapse have been introduced in the literature [24,25]. However, fragility curves and the collapse margin ratio (CMR) represent better criteria for such evaluations. In this study, the post-fire seismic behavior of intermediate MRFs (IMFs) at three height levels is investigated. The archetypes are exposed to fire scenarios defined for either single or multiple stories, addressing nearly all of the fire ignition possibilities. Moreover, structures are cooled down using different methods at system level with the aim of choosing the critical case. Time-history analyses are carried out under far-field (FF), near-field with pulse (NF-Pulse), and near-field without pulse (NF-No Pulse) seismic records. The incremental dynamic analyses were conducted in two directions via OpenSees 3.3.0 software. Finally, exceedance probabilities are calculated based on data from fragility analyses, and CMRs are drawn to determine the ultimate safety of fire-exposed structures in a future seismic event.

2. Materials and Methods

2.1. Assessment Procedure

Figure 1 illustrates the consecutive steps of current research. At the first stage, three steel structures with the IMF system were three-dimensionally designed via ETABS 9.7.4. software in accordance with the requirements of ASCE/SEI 7-16 [26]. To optimize computational resources, two-dimensional frames were selected from the investigated models and simulated in OpenSees software.

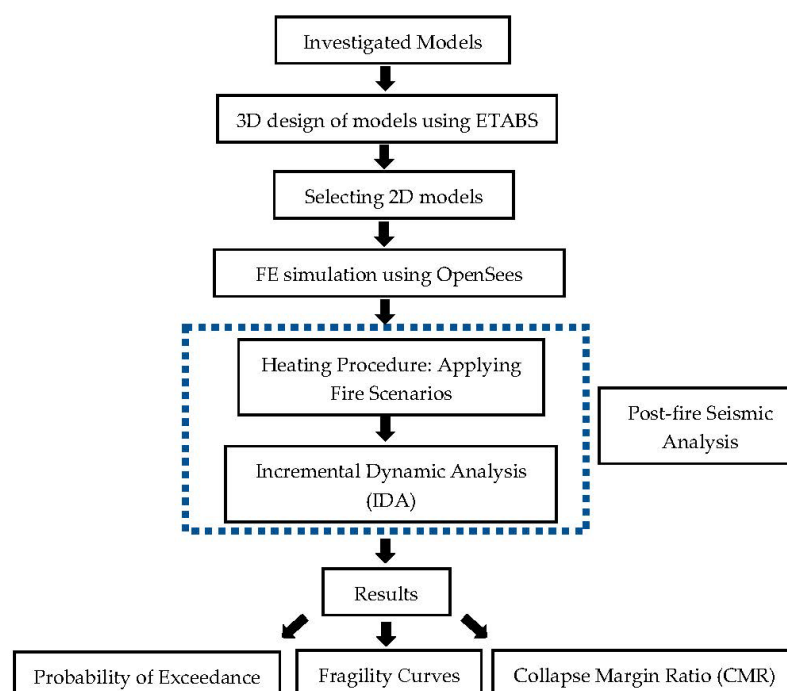


Figure 1. Assessment procedure for post-fire seismic analyses.

In the next step, a complete range of possible fire scenarios were planned and applied to FE models. Using FEMA-P695 [27] ground motion records, IDA analyses were carried out on both heated and unheated structures. Then, log-normally distributed seismic fragility curves of models were depicted as to which exceedance probabilities were calculated. Finally, margins of safety were determined according to FEMA-P695 [27].

2.2. Specifications of Archetypes

This research aims to gain a broader understanding of IMF seismic performance in multi-hazard fire scenarios due to their widespread use in many earthquake-prone areas. The reason for choosing the intermediate type of moment-frame is that such systems do not completely meet special detailing requirements for ductile behavior. Thus, IMF post-fire cases are more prone to seismic hazard. Since a lower percentage of research is carried out considering this system compared to special moment frames (SMF), the type of moment-resisting steel frame used in this study is the one with an intermediate level of ductility.

Investigated models consist of three multi-level steel IMFs of 3-, 6-, and 9-story buildings with modification factor (R) equal to 4.5, designed in ETABS software [28]. The design conforms to ASCE/SEI 7-16 [26] standard requirements. A region of high seismic intensity with risk and seismic design category of II and D, respectively, and associated parameters $S_s = 1.5 g$ and $S_1 = 0.6 g$ is supposed. The structures are designed for the soil class C, with 360 m/s shear velocity. Structural steel has the yield and ultimate strengths of 240 MPa and 370 MPa, respectively. In addition, its modulus of elasticity and ultimate strain equal to 2.0×10^5 MPa and 0.25, respectively. The columns are rigidly restrained at the position of supports, and strip foundation is designed separately. The archetypes are identical to the previous work of authors, and a full description of the designed cross-sections is given in the referenced paper [29].

Figure 2 illustrates the geometrical configuration of the models. The rectangular plan is similar in all structures with dimensions of 25×15 m. Span lengths in both directions are typically 5 m. According to the plan view, three moment frames on each side of the perimeter form the lateral force-resisting system of buildings, with gravity frames composing inner parts. Furthermore, the height of all stories is identically considered as 3.2 m.

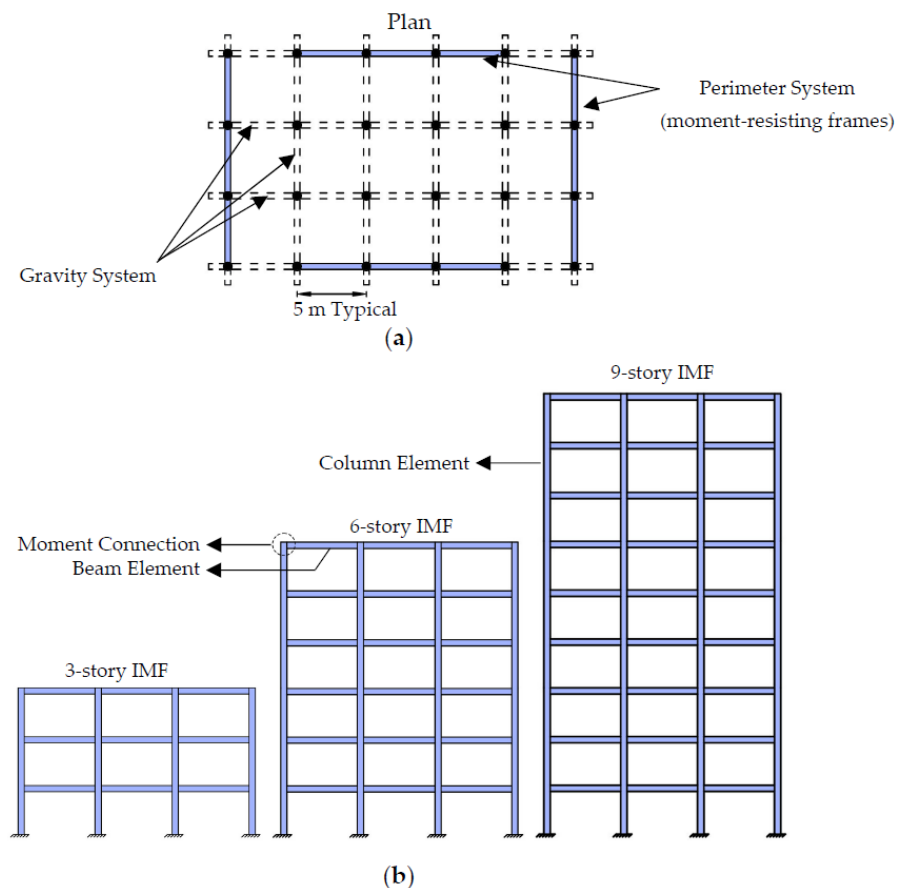


Figure 2. Configuration of models: (a) Typical Plan; (b) Elevation of structures.

2.3. Fire Scenarios

As mentioned in the Section 1, the level of damage followed by fire incident determines whether the structure can be accommodated or the cost of repair is uneconomical. Since the first two states are more prevalent among fire-affected MRFs, to estimate residual stress in structural component is inevitable. This goal can be achieved by conducting experimental tests on the target grade of steel under different peak temperatures and cooling methods.

Herein, the values of degenerated mechanical properties are granted from the experimental tests on various steel types [30]. The test results served as the benchmark for material simulation of heated models. Since this study deals with fire conditions with maximum recorded temperature of 800 °C and 1000 °C and cooling methods of air and water, the mechanical properties were directly obtained according to the predictive formulations presented in the referenced research paper (See Table 1). In addition, Figure 3 illustrates the post-fire stress–strain curves of the steel material for different variations.

Table 1. Post-fire mechanical properties at two elevated temperatures.

Steel Type	Temperature (°C)			
	800		1000	
	Cooling Method			
	Air	Water	Air	Water
E (MPa)	2.0×10^5	2.0×10^5	1.8×10^5	1.9×10^5
f_y (MPa)	213.5	224	171	201
f_u (MPa)	348	365.6	321.5	363
ε_y (-)	0.001	0.001	0.0009	0.001
ε_u (-)	0.20	0.21	0.19	0.2
ε_p (-)	0.19	0.16	0.18	0.13

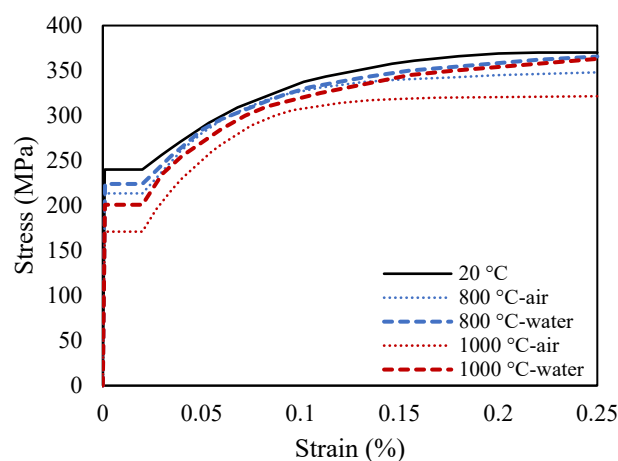


Figure 3. Stress–strain curve of steel material at the elevated temperatures.

In FE models, the simulation of fire is carried out by reducing the initial mechanical properties to the values of degenerated material. To apply degraded parameters to the models, different fire scenarios were devised to address the inherent randomness in spread of fire within their stories. Three factors were considered in the selection of a fire scenario for each model, including the location of fire exposure, cooling methods, and peak temperature. The number of scenarios under which the 3-, 6-, and 9-story IMFs were analyzed was, sequentially, 16, 24, and 24, which forms a total of 64 fire scenarios. Table 2 shows the full description of undertaken scenarios, by which the two-dimensional FE models are differentiated. The acronyms appear in this order: total number of stories, fire-exposed levels, peak temperature, and cooling method, which is either air (a) or water (w). For instance, MRF03-1to3-800w is the model with a 3-story whose total stories are subjected to

800 °C heating and are subsequently cooled down by water. Figure 4 shows the fire scenario in a 3-story IMF when the affected stories comprise only the second floor (Figure 4a) and all three story levels (Figure 4b).

Table 2. Description of fire scenarios.

Structure	Stories Exposed to Fire	Temperature (°C)			
		800		1000	
		Cooling Method			
		Air	Water	Air	Water
3	1st	MRF03-1-800a	MRF03-1-800w	MRF03-1-1000a	MRF03-1-1000w
	2nd	MRF03-2-800a	MRF03-2-800w	MRF03-2-1000a	MRF03-2-1000w
	3rd	MRF03-3-800a	MRF03-3-800w	MRF03-3-1000a	MRF03-3-1000w
	1st to 3rd	MRF03-1to3-800a	MRF03-1to3-800w	MRF03-1to3-1000a	MRF03-1to3-1000w
6	1st + 2nd	MRF06-1to2-800a	MRF06-1to2-800w	MRF06-1to2-1000a	MRF06-1to2-1000w
	2nd + 3rd	MRF06-2to3-800a	MRF06-2to3-800w	MRF06-2to3-1000a	MRF06-2to3-1000w
	3rd + 4th	MRF06-3to4-800a	MRF06-3to4-800w	MRF06-3to4-1000a	MRF06-3to4-1000w
	4th + 5th	MRF06-4to5-800a	MRF06-4to5-800w	MRF06-4to5-1000a	MRF06-4to5-1000w
	5th + 6th	MRF06-5to6-800a	MRF06-5to6-800w	MRF06-5to6-1000a	MRF06-5to6-1000w
	1st to 6th	MRF06-1to6-800a	MRF06-1to6-800w	MRF06-1to6-1000a	MRF06-1to6-1000w
9	1st to 3rd	MRF09-1to3-800a	MRF09-1to3-800w	MRF09-1to3-1000a	MRF09-1to3-1000w
	3rd + 4th	MRF09-3to4-800a	MRF09-3to4-800w	MRF09-3to4-1000a	MRF09-3to4-1000w
	4th to 6th	MRF09-4to6-800a	MRF09-4to6-800w	MRF09-4to6-1000a	MRF09-4to6-1000w
	6th + 7th	MRF09-6to7-800a	MRF09-6to7-800w	MRF09-6to7-1000a	MRF09-6to7-1000w
	7th to 9th	MRF09-7to9-800a	MRF09-7to9-800w	MRF09-7to9-1000a	MRF09-7to9-1000w
	1st to 9th	MRF09-1to9-800a	MRF09-1to9-800w	MRF09-1to9-1000a	MRF09-1to9-1000w

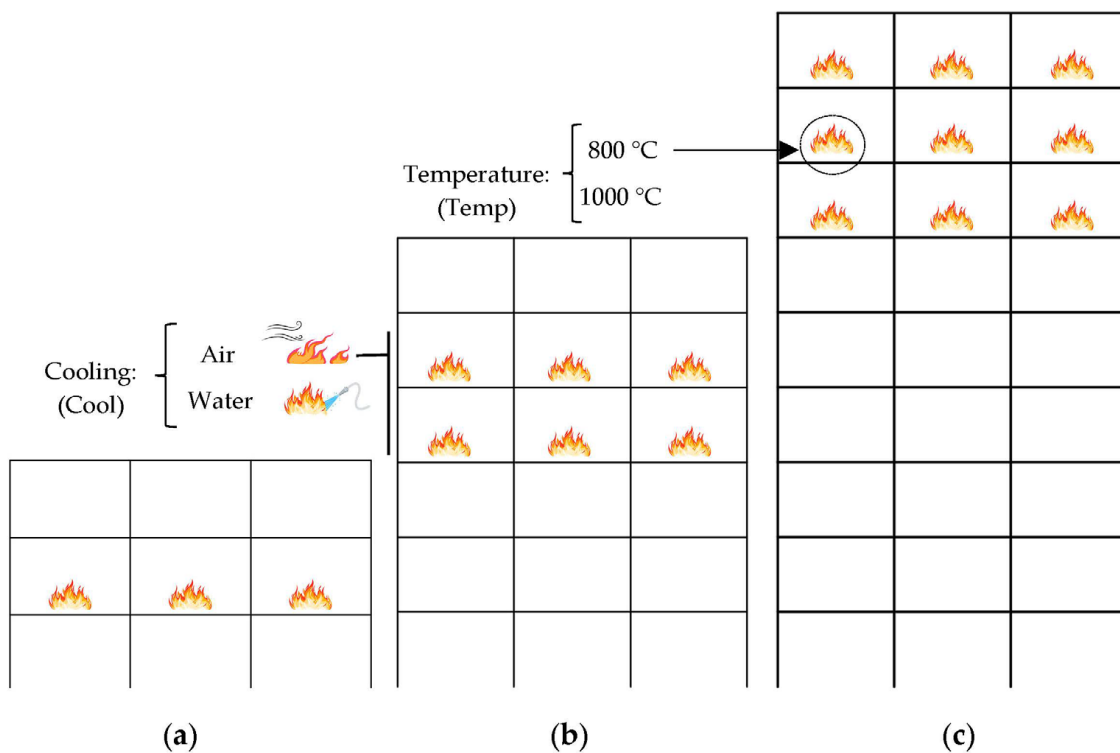


Figure 4. Scheme of the fire scenarios; (a) [MRF03-2-Temp-Cool]; (b) [MRF06-4to5-Temp-Cool]; (c) [MRF09-7to9-Temp-Cool].

2.4. Numerical Simulation

To save computational resources, a two-dimensional moment-resisting frame with each joint having three degrees of freedom has been chosen from each model and simulated using OpenSees's [31] finite element software with the same boundary condition and gravity loading as the initial design. The gravity load combination for nonlinear procedures was set to $1.05DL + 0.5LL$ based on a research study [32]. To achieve more reliable results, total frame mass is calculated at story level and assigned to concentrated nodes. A set of P- Δ columns, also known as the leaning column, with two-force members are simply linked to the two-dimensional frame via a "truss" element to simulate the lateral load induced by the mass of inner frames (Figure 5). The P- Δ columns are modeled using rigid elements. The practice of such a measure to capture additional deflection demands is encouraged in many studies [33–35]. The hysteretic behavior of structural steel is modelled using "uniaxialMaterial Steel02", featuring isotropic strain hardening and degradation of material. Additionally, the steel structural components were assigned "Nonlinear forceBeamColumn" elements, considering 10 integration points along the element. Numerical integration utilizes the Gaussian quadrature rule. Sections are simulated via "FiberSection" object, with a structured mesh size of $1 \times 1 \text{ cm}^2$ for web and $0.5 \times 0.5 \text{ cm}^2$ for flange. The choice of mesh size was inspired by the work of Quayyum et al. [15].

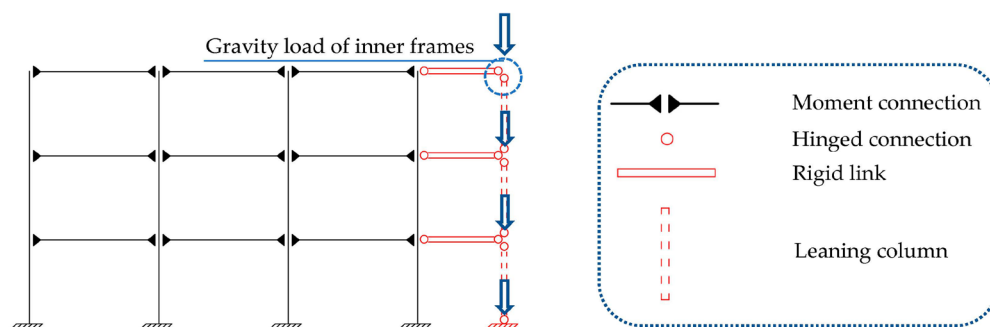


Figure 5. Illustration of P- Δ column in 3-story FE model.

A reliable constitutive model of post-fire structure requires inputting degraded mechanical properties of steel according to the predictive equations and the resulting stress–strain curves. At this stage, steel material properties are applied to fire scenario models. Two groups were considered: initial and post-fire cases. The initial cases consist of models with the primary mechanical properties of steel at ambient temperature, while those of post-fire cases vary with fire scenarios. In OpenSees, steel material was assigned to structural elements using uniaxial Giuffre–Menegotto–Pinto steel with isotropic strain hardening, which features cyclic degradation. It must be mentioned that the verification of the numerical modeling has been performed based on the available experimental data [36] and that these results are reported elsewhere [29].

2.5. Time-History Analysis

2.5.1. Record Selection

Many approaches have been offered in the literature to model the plastic behavior of steel structures using Non-Linear Time-History Analysis (NLTHA) [37]. NLTHA is carried out in the current work under three sets of ground motion records. A total of 50 record sets were selected from the Appendix-A of FEMA-P695 [27], including 22 far-field (FF), 14 near-field with pulse (NF-Pulse), and 14 near-field without pulse (NF-No Pulse) earthquakes. The description of the main parameters of record sets is presented in Table 3.

Table 3. Specification of PGA and PGV for record sets.

Record Type	PGA (g)			PGV (cm/s)			Distance ** (km)		
	Min.	Max.	Ave. *	Min.	Max.	Ave.	Min.	Max.	Ave.
FF	0.21	0.82	0.43	19	115	46	11.7	35.5	18.5
NF-Pulse	0.22	0.87	0.53	29.8	169.3	98.99	3.5	10.8	6.17
NF-No Pulse	0.28	1.43	0.65	34.7	126.4	80.1	3.9	12.1	7.6

* Ave. is Average. ** Distance refers to Campbell site-source distance criteria.

2.5.2. Development of Fragility Curves

To evaluate the seismic responses of a building thoroughly, Incremental Dynamic Analysis (IDA) has been proposed. This involves subjecting structural models to multiple records scaled with different seismic intensity levels ranging up to the collapse of system. The ground motion records are scaled to their unique $S_{a,T1}$ value, defined as the spectral acceleration corresponding to the first mode of the system with 5% damping ratio, and selected as the Intensity Measure (IM) to form the input of IDA analysis; the maximum inter-story drift ratio is chosen as Engineering Demand Parameter (EDP).

The resulting set of IDA curves are further analyzed to generate fragility curves. The fragility curves are rational means of predicting potential damage of structure during earthquake and determine the susceptibility of a member or system to meet the PL thresholds. Currently, the Hazus manual [38] represents criteria for seismic loss estimation and a benchmark from which damage limit states can be derived. According to Hazus, for a given level of structural response, fragility curves distribute damage between four physical damage states: Slight (S), Moderate (M), Extensive (E), and Complete (C). Table 4 shows the corresponding values of PLs for the investigated structures.

Table 4. Percentage of drift ratio for high-code design level [38].

Structures	Drift Ratio of Damage State Levels			
	S	M	E	C
3-story	0.6	1.2	3.0	8.0
6-story	0.4	0.8	2.0	5.33
9-story	0.3	0.6	1.5	4.0

The probability of EDPs exceeding a given PL can be demonstrated by a lognormal cumulative distribution function. The probability of a ground motion exceeding a given PL, C , at a particular IM , X , can be modeled as [39]:

$$P(C|IM = X) = \Phi\left(\frac{\ln\left(\frac{x}{\theta}\right)}{\beta}\right), \quad (1)$$

$$\ln(\theta) = \frac{1}{n} \sum_{i=1}^n \ln(IM_i). \quad (2)$$

$$\beta = \sqrt{\frac{1}{n-1} \sum_{i=1}^n \left(\ln\left(\frac{IM_i}{\theta}\right)\right)^2} \quad (3)$$

where $\Phi(\cdot)$ is the standard normal cumulative distribution function (CDF), θ is the median of the fragility function, β is the standard deviation of $\ln IM$, n is the total number of earthquake records considered, and IM_i is the value of IM at which a certain PL is exceeded in the i th ground motion. Considering the given limit states in Table 4 and data from IDA analysis, fragility curves are derived.

2.5.3. Collapse Margin Ratio

The procedure to identify a collapse point under individual intensities of ground motion was described in the previous section. The term “Median Collapse Capacity”, \hat{S}_{CT} , corresponds to the spectral intensity with 50% probability of collapse. Calculating \hat{S}_{CT} involves scaling all the ground motions to MCE intensity, S_{MT} . Then, the intensities are increased until the structural collapse occurs under over half of the scaled records. The lowest intensity at which this objective is accomplished is selected as \hat{S}_{CT} . Furthermore, S_{MT} is defined as the intensity corresponding to the fundamental vibration period of the structure and is obtained from the MCE response spectrum. Collapse safety of the structure is mainly characterized by a parameter called the Collapse Margin Ratio (CMR) and is described by the ratio between \hat{S}_{CT} and S_{MT} (Equation (4)) which is necessarily equal to or greater than 1 [40].

$$\text{CMR} = \frac{\hat{S}_{CT}}{S_{MT}}, \quad (4)$$

Collapse fragility curves can be obtained using the cumulative distribution function (CDF) of collapse data points from IDA curves and fitting a lognormal distribution. Since this is a demanding task, the full IDA process is unnecessary in studies whose only aim to capture a CMR value. Thus, a fewer number of analyses may be required after selecting the intensities close to the expected one. However, the number of increased intensities should be sufficiently enough to confirm the suitability of the method.

3. Results

3.1. IDA Curves

IDA plots present the result of each nonlinear analysis in terms of the spectral intensity of the earthquake (IM) on the vertical axis versus the corresponding result for the recorded maximum inter-story drift ratio (DM) on the horizontal axis. The results of a given record scaled to increasing spectral intensities are connected through a line. Different ground motions generate varying results in the same index, according to the inherent differences in their frequency content. Collapse assessment is judged either directly or indirectly as stated in Chapter 6 of FEMA-P695 [27].

IDA response plots for three structural models are depicted in Figures 6–8, each representing a comparison between a heated scenario and initial archetype in a given set of records. The post-fire scenario in all three heights indicates the one in which all stories are affected by 1000 °C temperature and the fire has naturally died out. In this work, collapse points are identified in 10% drift ratio, which is approved in performance-based seismic design literature to be a reasonable collapse criterion [29,40]. The corresponding $S_{a(T1,5\%)}$ at collapse point in the 50% fractile IDA curves is approximately 2.0 g, except for NF-Pulse records with nearly 1.7 g spectral acceleration at 10% drift ratio. Different records provide dispersed results. However, DM is a monotonic function of IM in the summary of IDA curves (i.e., 16%, 50%, and 84% fractile IDAs) without displaying a twisting pattern. These figures indicate that there is an inverse relationship between height and maximum spectral intensity in the collapse point which is evidenced by the lower slope of plots in the 9-story structure compared to the others.

Another common trend is the impact of FF records on 50% percentile IDA among identical models. The FF ground motions should be scaled up to marginally higher spectral intensities to reach collapse point, which indicates that near-field records have more devastating impacts on archetypes due to their high frequency content. This is more evident in 3-story structures, especially in NF-Pulse records. Comparing the IDA fractile curves, it is observed that when S_a is less than 0.5 g, the values of 16%, 50%, and 84% percentiles almost coincide, and post-fire condition has no noticeable effect on the structure. However, as S_a increases, the diversion between percentiles also amplifies, making the effect of fire clear and significant.

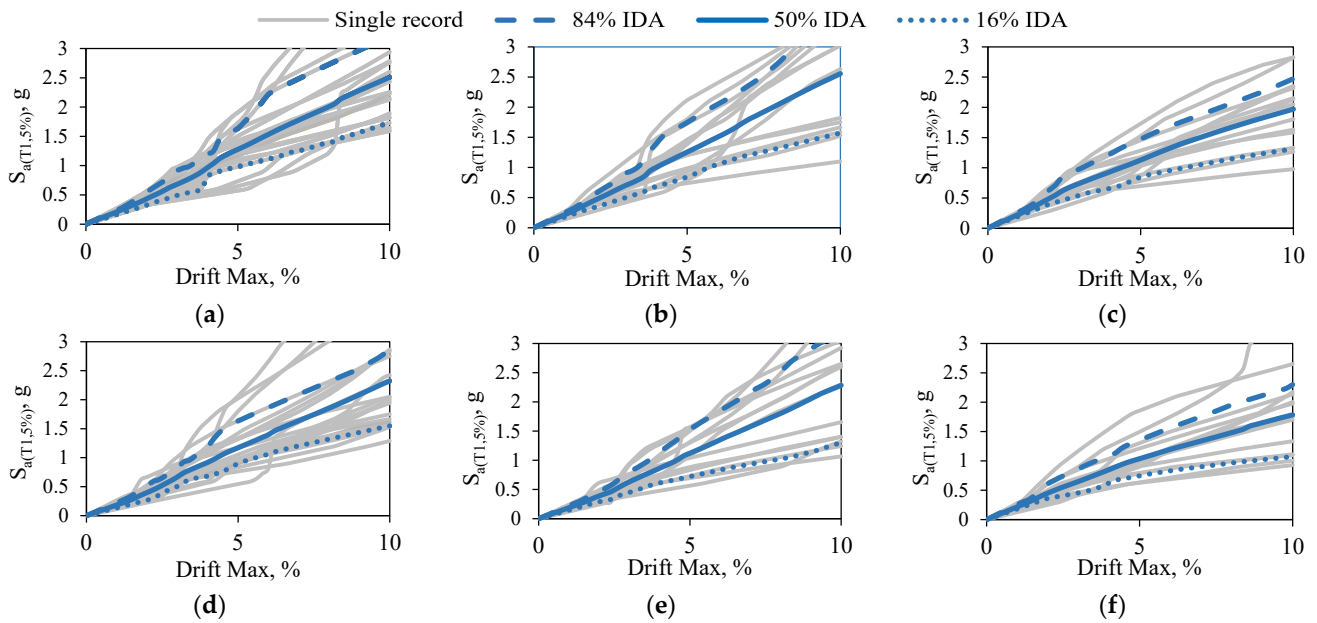


Figure 6. The 16%, 50%, and 84% fractile IDAs for 3-story initial and MRF03-1to3-1000a scenario models subjected to (a,d) FF, (b,e) NF-No Pulse, and (c,f) NF-Pulse records, respectively.

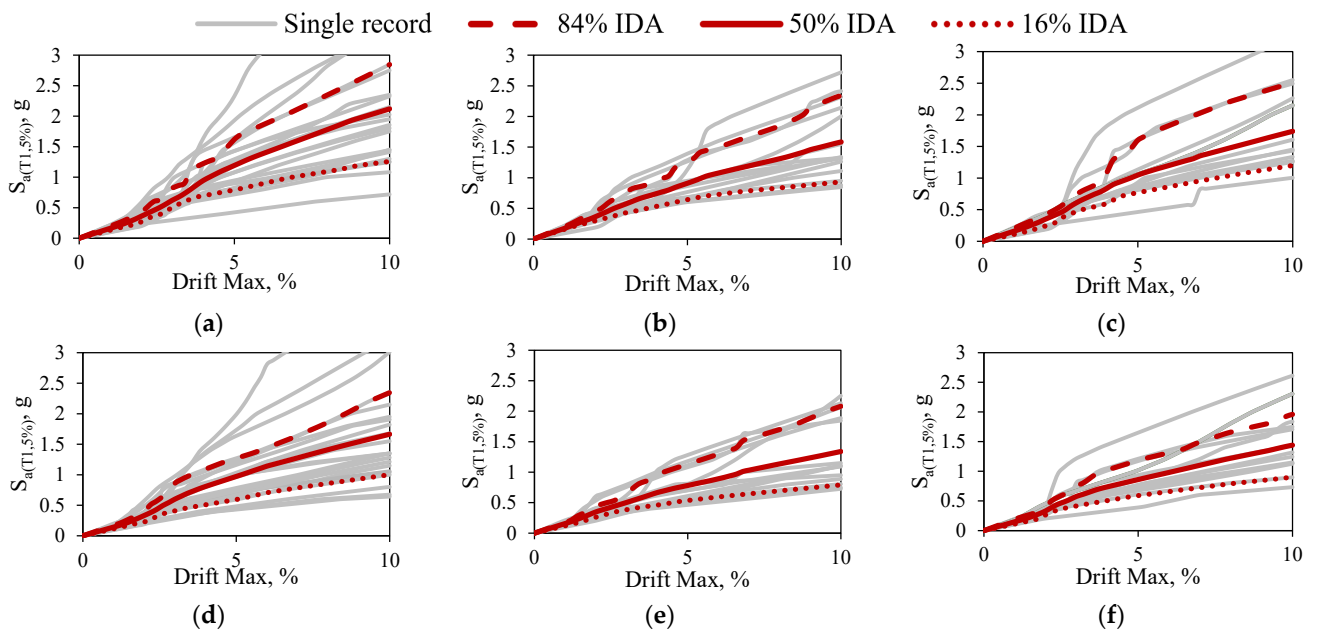


Figure 7. The 16%, 50%, and 84% fractile IDAs for 6-story initial and MRF06-1to6-1000a scenario models subjected to (a,d) FF, (b,e) NF-No Pulse, and (c,f) NF-Pulse records, respectively.

3.2. Fragility Curves

Figures 9–11 show the fragility curves of each model under different earthquake records in heated and unheated conditions. The selected post-fire scenario is the same as the one presented in the IDA results. For a given PL, the Probability of Failure (POF) in a given spectral acceleration is pointed and fitted by a lognormal distribution.

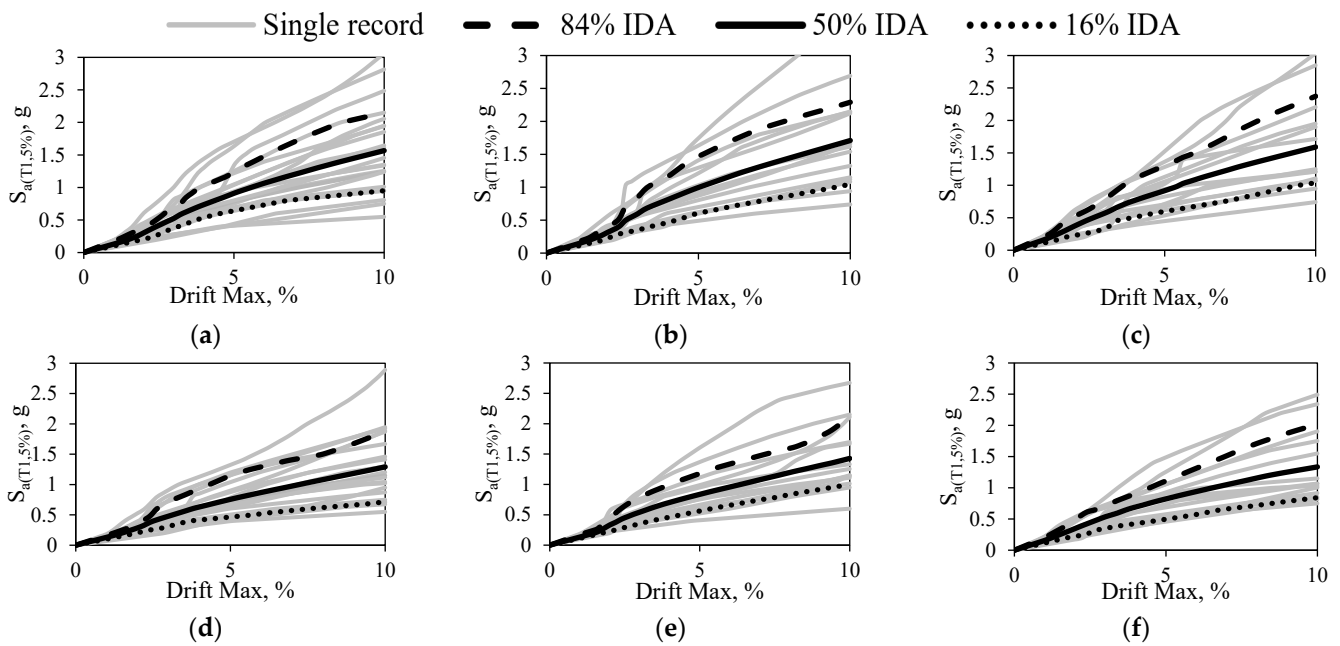


Figure 8. The 16%, 50%, and 84% fractile IDAs for 9-story initial and MRF09-1to9-1000a scenario models subjected to (a,d) FF, (b,e) NF-No Pulse, and (c,f) NF-Pulse records, respectively.

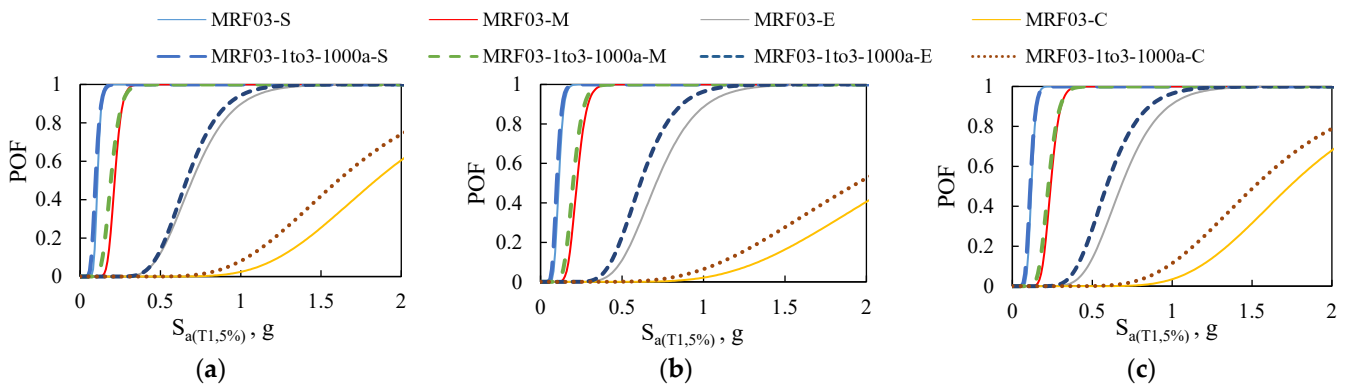


Figure 9. Fragility curves of 3-story structure subjected to (a) FF, (b) NF-No Pulse, and (c) NF-Pulse records, respectively.

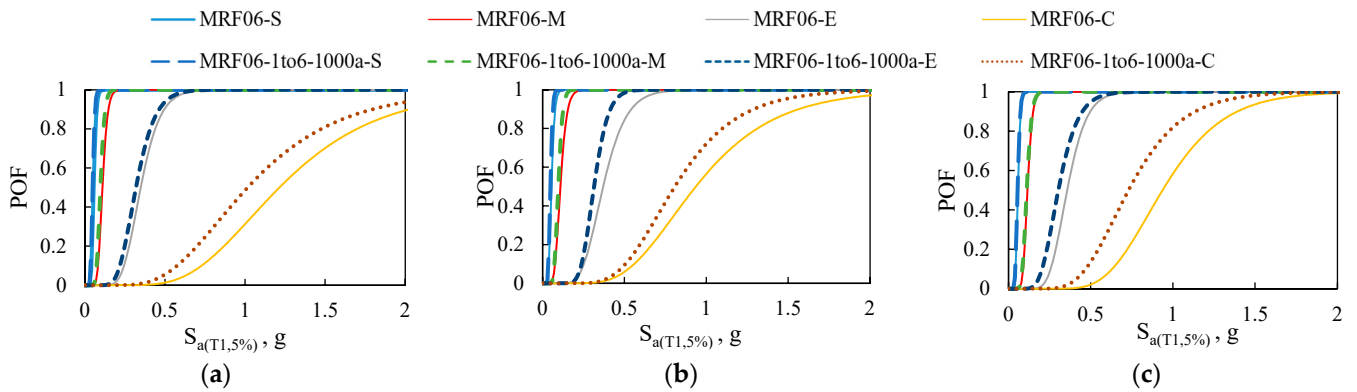


Figure 10. Fragility curves of 6-story structure subjected to (a) FF, (b) NF-No Pulse, and (c) NF-Pulse records, respectively.

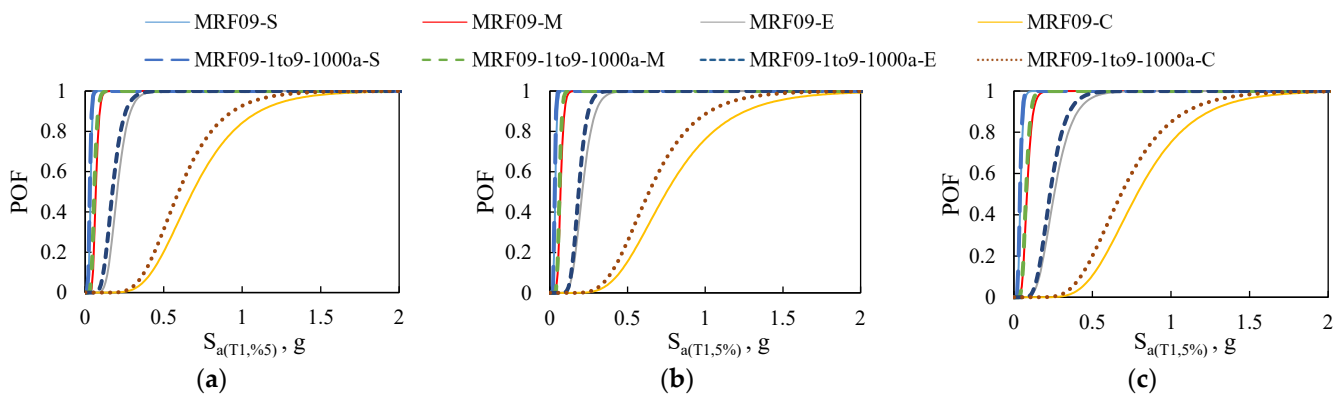


Figure 11. Fragility curves of 9-story structure subjected to (a) FF, (b) NF-No Pulse, and (c) NF-Pulse records, respectively.

Generally, earthquakes following fire has an apparent effect on the performance of all frames at different PLs. The increase in the height of the structure raises its vulnerability to seismic loading after a fire incident. The POFs for post-fire and the initial case in the spectral acceleration at the fundamental period, $S_{a(T1)}$, are computed to be 0.52 and 0.45 in the E damage level of Figure 9a, respectively. According to Figure 10a, the related measures for 6-story structures are 0.9 and 0.86, respectively. Therefore, the POF in $S_{a(T1)}$ and for a given PL increases with the increase in the height of the structure. In contrast, temperature-conditioned structures decrease \hat{S}_{CT} more prominently with the decrease in structural height. With regard to the suites of records, the structures of 3- and 6-story structures revealed the minimum POF when subjected to FF ground motions, while such records generated the maximum POF in 9-story structures.

Although previous fire exposure marginally altered the slight, moderate, and extensive damage states of the unheated archetypes in their $S_{a(T1)}$, it imposed great impact on the POF in the complete damage state, particularly in the 6-story structure. It is evidenced from Figure 10c with a relatively 8.8% increase in POF, where only 0.8% and 2.7% is captured for the 3- and 9-story structures, respectively. According to Figure 9, POF in $S_{a(T1)}$ and at the extensive damage level of initial structures subjected to FF, NF-No Pulse, and NF-Pulse records were 44%, 42%, and 47%, respectively, while the corresponding values for the 6- and 9-story structures were almost twice as much. However, less than 5% probability of exceedance at $S_{a(T1)}$ from damage state C was drawn for all of the initial structures.

3.3. Inter-Story Drift Ratio

In this section, median inter-story drift ratios under $S_{a(T1,5\%)}$ corresponding to 50% POF of each PL are withdrawn and illustrated in Figures 12–14. Using data from the fragility analysis, individual ground motion records are scaled to the median spectral acceleration of each PL. Afterwards, each structure is seismically analyzed in its initial and critical fire scenario, and the median drift ratio of the entire record set is determined for each story level. The reason to select median $S_{a(T1,5\%)}$ at each PL is that this is assumed to be the representative of spectral acceleration of the structure after a seismic event. Therefore, the resulted maximum drifts marginally vary with the drift ratio limits of PLs.

Generally, inter-story drift ratios are lower in fire-exposed structures than the initials, except for the stories where fire was ignited. This trend is confirmed in almost all structures, such as in Figure 14 where only the 4th story drift ratio in heated models transcended that of initial structures.

In the 3-story structure, inter-story drift ratios almost remained steady between initial and critical fire scenarios in the S and M levels. However, the difference increased significantly with the increase in PL. In addition, the roof level in which the fire had been initiated in the critical scenario demonstrated higher percentages of drift in all sets of records. Since the entire levels of the 6-story structure were elevated in its critical fire scenario, its profile

drift ratio was constant in both heated and unheated models. The first three PLs also showed a good agreement, particularly in FF records, yet the drift ratios at C level varied in the same manner. In the 9-story structure, the influence of fire was obvious in the 4th story with a 0.6% increase in drift percentage. With regard to earthquake records, NF-Pulse, FF, and NF-No Pulse had the most impact in the 3-, 6- and 9-story structures, respectively.

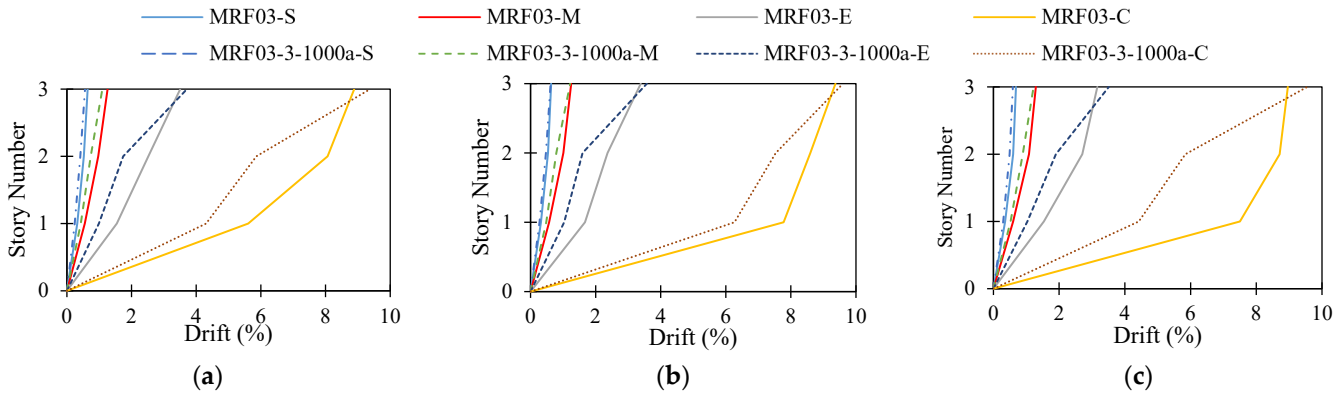


Figure 12. Inter-story drift ratios for 3-story structure subjected to (a) FF, (b) NF-No Pulse, and (c) NF-Pulse records, respectively.

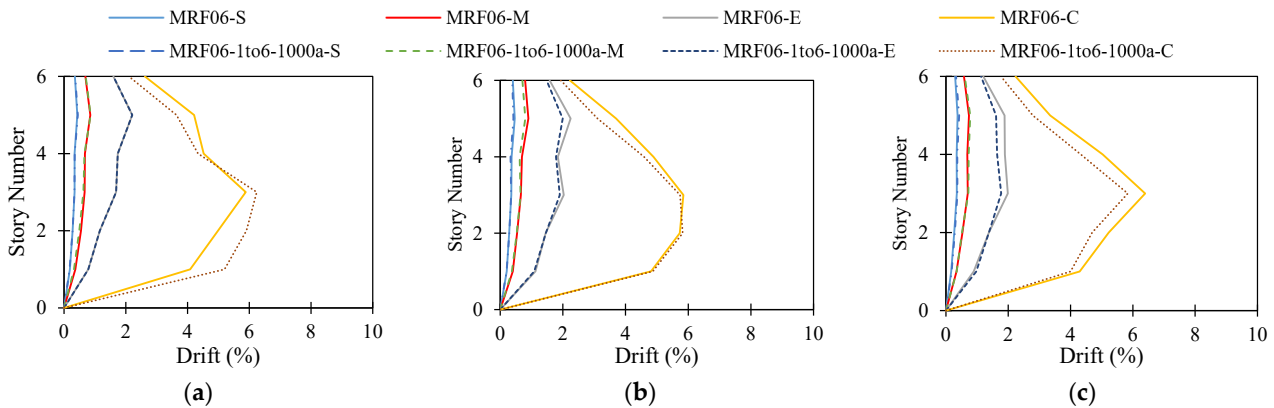


Figure 13. Inter-story drift ratios for 6-story structure subjected to (a) FF, (b) NF-No Pulse, and (c) NF-Pulse records, respectively.

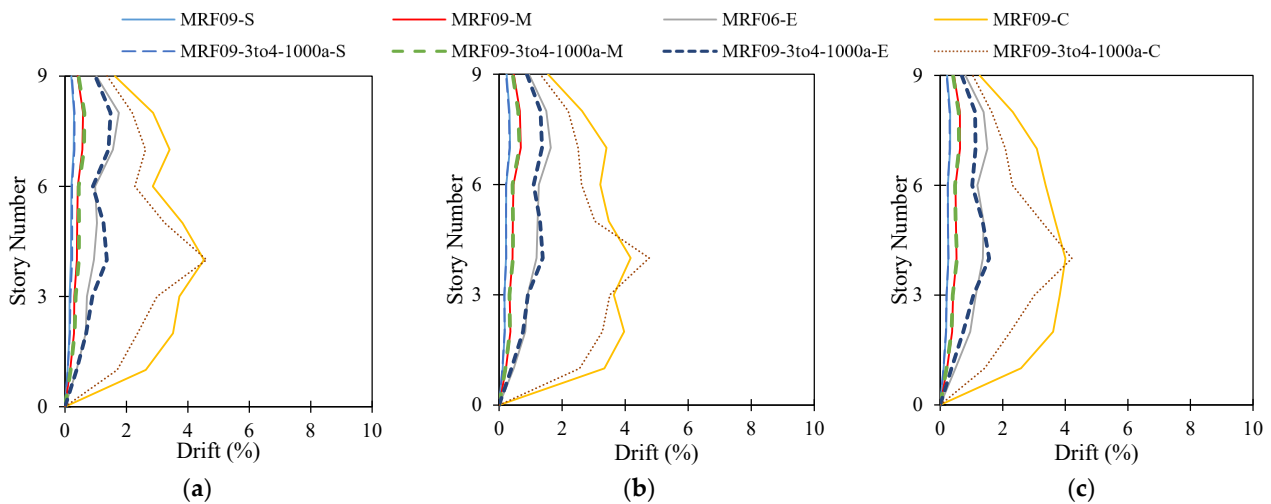


Figure 14. Inter-story drift ratios for 9-story structure subjected to (a) FF, (b) NF-No Pulse, and (c) NF-Pulse records, respectively.

3.4. Exceedance Probability at $S_{a(T1)}$

The probability of exceedance defines the extent at which the scenario model is predicted to exceed the damage state limits in the spectral acceleration of the structure in accordance with the design level. This is obtained from statistical data of the fragility curves. By processing the data from fragility analyses, it was observed that different cooling methods in a similar fire scenario were so scattered and random that no trend could be determined. In addition, the case was the most severe in all models when the entire story levels had been previously heated.

Table 5 compares the probability of exceedance from damage state levels at $S_{a(T1)}$ between the initial FE models and the average of fire-exposed structures. From the table, higher exceedance probabilities are evident for fire-exposed frames at the same suit of ground motion records. Moreover, all cases exceed the moderate damage state, and there is an increase in the probability of exceedance from both extensive and complete levels in post-fire structures. This is more obvious in the 3-story structure subjected to NF-No Pulse records reaching from nearly 68% to 75% in the extensive damage level and 0.5% and 0.87% in the complete damage level.

Table 5. Comparison of exceedance probability in pre- and post-fire seismic event.

Scenario		FF (%)				NF-No Pulse (%)				NF-Pulse (%)			
		S	M	E	C	S	M	E	C	S	M	E	C
3-story	Initial	100.0	100.0	69.7	0.4	100.0	100.0	67.6	0.5	100.0	100.0	72.7	0.6
	PF *	100.0	100.0	74.14	0.77	100.0	100.0	75.19	0.87	100.0	100.0	77.53	1.44
6-story	Initial	100.0	100.0	91.4	1.4	100.0	100.0	85.5	6.4	100.0	100.0	91.2	2.4
	PF	100.0	100.0	91.9	2.5	100.0	100.0	89.7	7.6	100.0	100.0	93.7	5.8
9-story	Initial	100.0	100.0	99.5	7.0	100.0	100.0	98.9	5.3	100.0	100.0	88.2	2.7
	PF	100.0	100.0	99.4	9.7	100.0	100.0	99.3	7.0	100.0	100.0	91.6	5.2

* PF stands for Post-Fire.

3.5. CMR Results

Figure 15 presents the summary of CMR data through comparative bar charts. Each set of three vertical bars relates to the collapse data from IDA analysis of an individual fire scenario under different record sets. Although FF records generated highest CMR in the 6-story structure, NF-No Pulse demonstrated the greatest values in the other two structures. Similarly, in all structures, the lowest margins of safety were captured when they were subjected to pulse-like frequency content. In 3-, 6-, and 9-story models, CMR peaked at around 2.4, 2.5, and 2.7, respectively. This underlines the direct relationship between height and safety.

In 3-, 6-, and 9-story structures, the most critical fire scenarios were MRF03-3-1000a, MRF06-1to6-1000a, and MRF09-3to4-1000a, respectively. The average CMR results of three record sets for the critical scenarios were around 17–20% lower than their corresponding values in initial cases, and about 12–16% lower than the average CMR of all records for post-fire scenarios. In addition, about half of the fire scenarios showed closely identical average CMRs to unheated structures. This indicates that the fire-exposed structures can serve similar margins of safety to their primary condition in almost one-half of the cases.

By comparing different cooling methods and elevated temperatures in a given number of stories exposed to fire, it is perceived that the air-cooled structures at 1000 °C heating tend to produce the lowest CMRs. The difference between cooling methods is more obvious at 1000 °C. Take the 9-story structure as an example, where every level had experienced fire. When subjected to NF-No Pulse records, CMRs of air-cooled and water-cooled structures are computed to be 2.57 and 2.60 at 800 °C, and 2.04 and 2.33 for 1000 °C temperature, respectively. Thus, only a reduction of 0.03 in CMR is observed at 800 °C compared to 0.27 at 1000 °C. The most critical scenarios also emphasize the deteriorating effect of air cooling which leads to a reduction in the total safety of the structures.

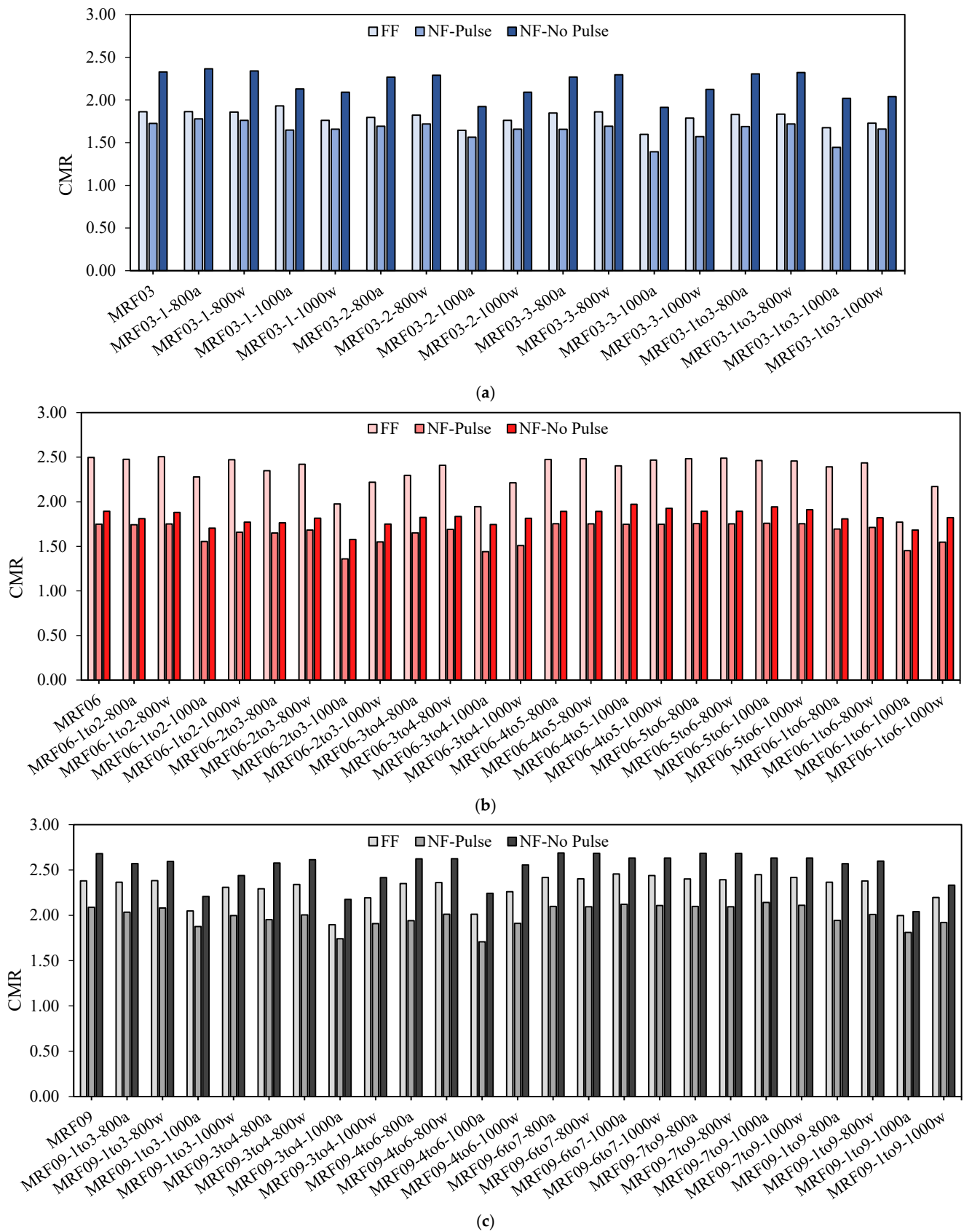


Figure 15. Calculation of CMR for two-dimensional frames of: (a) 3-story; (b) 6-story; (c) 9-story structure.

Table 6 compares the values of CMR for the average and critical post-fire structures with initial cases in terms of reduction percentages. A general decrease in measures can be observed in temperature-conditioned structures. For instance, the CMRs of 3-, 6-, and 9-story IMFs subjected to far-field records were computed to be 1.86, 2.50, and 2.38, while these values for the post-fire ones dropped to 1.79, 2.34, and 2.30, respectively. Considering the mean post-fire structures, a maximum decrease of 7.4% in CMR can be observed in the 3-story structures subjected to NF-No Pulse ground motions. Although the mean fire scenarios reduced CMR by less than 10%, the reduction in measures at the most critical fire scenarios ranged between 12.5% and 41.2%.

Table 6. Comparison of CMR.

Scenario		FF	% **	NF-No Pulse	%	NF-Pulse	%	Avg. ***	%
3-story	Initial	1.86		2.33		1.73		1.97	
	PF *	1.79	−3.9	2.17	−7.4	1.64	−5.5	1.87	−5.3
	PF _c *	1.60	−16.2	1.91	−22.0	1.39	−24.5	1.63	−20.9
6-story	Initial	2.50		1.89		1.75		2.05	
	PF	2.34	−6.8	1.82	−3.8	1.65	−6.1	1.94	−5.7
	PF _c	1.77	−41.2	1.68	−12.5	1.45	−20.7	1.64	−25.0
9-story	Initial	2.38		2.68		2.09		2.38	
	PF	2.30	−3.5	2.52	−6.3	1.99	−5.0	2.27	−4.8
	PF _c	1.90	−25.3	2.18	−22.9	1.74	−20.1	1.94	−22.7

* PF and PF_c are the mean and critical Post-Fire CMRs, respectively. ** % is the percentage of decrease in post-fire response. *** Avg. is the average of three records.

The lowest safety level of the structure was observed when subjected to NF-Pulse records. That is to say, the corresponding values of mean CMR are significantly lower than their counterparts from different record sets. This shows the structural vulnerability to pulse-like characteristics of ground motions and should be addressed clearly in the design stage of buildings in regions of moderate to high seismicity.

4. Conclusions

Previous research can only be considered a first step towards a more profound understanding of post-fire seismic performance of steel frames. However, there is much unknown about the behavior of such fire-exposed structures with the IMF system during a future seismic event. The post-fire seismic assessment of IMFs is of significant importance due to their vulnerability to collapse after degradation of mechanical properties. In this paper, archetypes that comprise 5-bay IMFs, with three different heights of 3, 6, and 9 stories, were seismically designed. Afterwards, perimeter two-dimensional frames with a lateral load-bearing system were selected and simulated in OpenSees software.

Considering a range of possible fire scenarios is the key criterion to determining the most severe case of a post-fire structure. Three variants were adopted to simulate different fire conditions, including peak temperature, cooling method, and the fire-affected stories. The FE models were categorized based on these fire scenarios. In addition, three sets of ground motion records with different site characteristics were selected from FEMA-P695 reference manual and scaled to increasing intensities. By conducting IDA analyses, fragility curves and the exceedance probability from damage state levels at the design spectral acceleration were obtained. Finally, the safety of structures was investigated by calculation of the Collapse Margin Ratio (CMR) for each model. Some major findings are summarized as follows:

- Investigating the comparative fragility curves, a greater POF can be seen with increasing the height of structures. This can be illustrated by the probability of extensive failure at $S_{a(T1)}$ for the initial 3-, 6-, and 9-story structures subjected to NF-No Pulse ground motions which equals to 42%, 78%, and 96%, respectively. Moreover, the

9-story structures subjected to NF-Pulse records are predicted to demonstrate earlier failures at their complete damage level, whereas the 3- and 6-story structures are the most susceptible to FF ground motions.

- Inter-story drift ratios were lower in the critical fire scenarios compared to the initial cases except for the stories affected by fire. For example, in the 3-story structure subjected to NF-Pulse records, drift ratio differed nearly 0.25% between the 2nd and 3rd stories of the initial model. However, the difference was 3.7% in the critical fire scenario, exceeding the roof drift ratio of the initial model. In addition, the 6-story structure showed the least variations in terms of drift percentage among all the studied structures due to its critical fire scenario.
- The CMR results show that the structures carry the lowest margins of safety when subjected to NF-Pulse records. This emphasizes the fact that pulse-like frequency contents reduce safety regardless of structural height. The minimum CMR values of NF-Pulse records in 3-, 6-, and 9-story structures were 1.39, 1.36, and 1.71, respectively.
- The air cooling method and the 1000 °C elevated temperature were found to exacerbate the seismic performance of post-fire structures. The CMR result for the most critical scenario in the 9-story structure, i.e., MRF09-3to4-1000a, subjected to NF-No Pulse ground motions was 2.18, while a value of 2.61 was determined for the fire scenario MRF09-3to4-800w.
- Generally, pre-exposing structures to fire decreases the margin of collapse safety compared to initial cases. This is evidenced by the average reduction percentages of CMR which are 20.9%, 25.0%, and 22.7% for the 3-, 6-, and 9-story structures in their most critical post-fire scenarios, respectively.

The findings of this study can contribute to a better understanding of seismic performance of steel structures which had previously experienced fire. In addition, CMR was found to be a key criterion to determine the capacity of post-fire structures. However, some limitations can be found within the content of this study including the ideal assumption of uniform distribution of temperature through steel members. Future research should be conducted in more realistic settings to validate the numerical conclusions of the current work. Researchers are recommended to perform thermal and thermomechanical analyses instead of deriving the post-fire mechanical properties from predictive equations. In such a case, the heterogeneity of residual stresses in structural components would be considered.

Author Contributions: E.M.D.: Conceptualization, Software, Methodology, Visualization, Investigation, Validation, Writing-Reviewing and Editing, Data curation. P.R.: Writing-Original draft preparation, Visualization, Investigation, Methodology. V.B.: Supervision, Methodology, Writing-Reviewing and Editing. A.S.: Conceptualization, Methodology, Validation, Investigation, Writing-Reviewing and Editing. F.A.: Investigation, Data curation, Writing- Reviewing and Editing. All authors have read and agreed to the published version of the manuscript.

Funding: This research was not funded by any funding bodies.

Data Availability Statement: Some or all data, models, or code that support the findings of this study are available upon reasonable request from the corresponding author.

Conflicts of Interest: The authors declare no conflict of interest.

References

1. EN 1998-1:2004; Eurocode 8: Design of Structures for Earthquake Resistance-Part 1: General Rules, Seismic Actions and Rules for Buildings. European Committee for Standardization: Brussels, Belgium, 2004.
2. Giuliani, L. Structural safety in case of extreme actions. *Int. J. Lifecycle Perform. Eng.* **2012**, *1*, 22–40. [[CrossRef](#)]
3. Outinen, J.; Mäkeläinen, P. Mechanical properties of structural steel at elevated temperatures and after cooling down. *Fire Mater.* **2004**, *28*, 237–251. [[CrossRef](#)]
4. Tao, Z.; Wang, X.Q.; Uy, B. Stress-strain curves of structural and reinforcing steels after exposure to elevated temperatures. *J. Mater. Civ. Eng.* **2013**, *25*, 1306–1316. [[CrossRef](#)]
5. Lee, J.; Engelhardt, M.D.; Taleff, E.M. Mechanical properties of ASTM A 992 steel after fire. *Eng. J.* **2012**, *49*, 33–44.

6. BS 5950; Structural Use of Steelwork in Building, Part 8: Code of Practice for Fire Resistant Design. British Standard Institution: London, UK, 1990.
7. Li, G.-Q.; Shou-Chao, J.; Yin, Y.-Z.; Chen, K.; Li, M.-F. Experimental studies on the properties of constructional steel at elevated temperatures. *J. Str. Eng.* **2003**, *129*, 1717–1721. [[CrossRef](#)]
8. Kirby, B.; Preston, R. High temperature properties of hot-rolled, structural steels for use in fire engineering design studies. *Fire Saf. J.* **1988**, *13*, 27–37. [[CrossRef](#)]
9. Maraveas, C.; Fasoulakis, Z.; Tsavdaridis, K.D. Post-fire assessment and reinstatement of steel structures. *J. Str. Fire Eng.* **2017**, *8*, 181–201. [[CrossRef](#)]
10. Priyadarshini, M.; Behera, A.; Biswas, C.K.; Rajak, D.K. Experimental analysis and mechanical characterization of AISI P20 tool steel through heat-treatment process. *J. Bio-Tribo-Corros.* **2022**, *8*, 1–10. [[CrossRef](#)]
11. Tide, R.H. Integrity of structural steel after exposure to fire. *Eng. J.-Am. Inst. Steel Constr.* **1998**, *35*, 26–38.
12. Smith, C.I.; Kirby, B.R.; Lapwood, D.G.; Cole, K.J.; Cunningham, A.P.; Preston, R.R. The reinstatement of fire damaged steel framed structures. *Fire Saf. J.* **1981**, *4*, 21–62. [[CrossRef](#)]
13. Kirby, B.; Lapwood, D.; Thomson, G. The reinstatement of fire damaged steel and iron framed structures. *Br. Steel Corp. Swinden Lab.* **1986**, *1986*, 79.
14. ASTM-A6; Standard Specification for General Requirements for Rolled Structural Steel Bars, Plates, Shapes, and Sheet Piling. American Society for Testing and Materials: West Conshohocken, PA, USA, 2011.
15. Quayyum, S.; Hassan, T. Seismic performance of a fire-exposed moment-resisting frame. *J. Str. Eng.* **2018**, *144*, 04018206. [[CrossRef](#)]
16. Wald, F.; Simões da Silva, L.; Moore, D.B.; Lennon, T.; Chladná, M.; Santiago, A.; Beneš, M.; Borges, L. Experimental behaviour of a steel structure under natural fire. *Fire Saf. J.* **2006**, *41*, 509–522. [[CrossRef](#)]
17. Rahnavard, R.; Thomas, R.J. Numerical evaluation of the effects of fire on steel connections; Part 1: Simulation techniques. *Case Stud. Therm. Eng.* **2018**, *12*, 445–453. [[CrossRef](#)]
18. Pantousa, D.; Karavasilis, T.; Maraveas, C. Numerical Investigation of the Post-Fire Performance of Steel Columns. *Buildings* **2022**, *12*, 288. [[CrossRef](#)]
19. Wang, G.-Y.; Zhang, C.; Xu, J.; Zhang, D.-M. Post-fire seismic performance of SRC beam to SRC column frames. *Structures* **2020**, *25*, 323–334. [[CrossRef](#)]
20. Mohebi, B.; Yazdanpanah, O.; Kazemi, F.; Formisano, A. Seismic damage diagnosis in adjacent steel and RC MRFs considering pounding effects through improved wavelet-based damage-sensitive feature. *J. Build. Eng.* **2021**, *33*, 101847. [[CrossRef](#)]
21. Taiyari, F.; Formisano, A.; Mazzolani, F.M. Seismic behaviour assessment of steel moment resisting frames under near-field earthquakes. *Int. J. Steel Str.* **2019**, *19*, 1421–1430. [[CrossRef](#)]
22. Sadeghi, A.; Kazemi, H.; Mehdizadeh, K.; Jadali, F. Fragility analysis of steel moment-resisting frames subjected to impact actions. *J. Build. Pathol. Rehabil.* **2022**, *7*, 26. [[CrossRef](#)]
23. Mazza, F.; Alesina, F. Fragility analysis of RC seismically-isolated structures with residual mechanical properties after fire exposure. *Soil Dyn. Eq. Eng.* **2019**, *121*, 383–398. [[CrossRef](#)]
24. Saadatmorad, M.; Talookolaei, R.-A.J.; Pashaei, M.-H.; Khatir, S.; Wahab, M.A. Pearson correlation and discrete wavelet transform for crack identification in steel beams. *Mathematics* **2022**, *10*, 2689. [[CrossRef](#)]
25. Ouladbrahim, A.; Belaidi, I.; Khatir, S.; Magagnini, E.; Capozucca, R.; Wahab, M.A. Prediction of Gurson damage model parameters coupled with hardening law identification of Steel X70 pipeline using neural network. *Met. Mater. Int.* **2022**, *28*, 370–384. [[CrossRef](#)]
26. ASCE/SEI 7-16; Minimum Design Loads and Associated Criteria for Buildings and Other Structures. American Society of Civil Engineers: Reston, WV, USA, 2017.
27. Applied Technology Council. FEMA P-695; Quantification of Building Seismic Performance Factors. Federal Emergency Management Agency (FEMA): Washington, DC, USA, 2009.
28. CSI Analysis Reference Manual for SAP2000, ETABS, and SAFE; Computers and Structures, Inc.: Walnut Creek, CA, USA, 2016.
29. Sabouniaghdam, M.; Mohammadi Dehcheshmeh, E.; Safari, P.; Broujerdian, V. Probabilistic collapse assessment of steel frame structures considering the effects of soil-structure interaction and height. *Sci. Iran.* **2022**, *29*, 2979–2994. [[CrossRef](#)]
30. Lu, J.; Liu, H.; Chen, Z.; Liao, X. Experimental investigation into the post-fire mechanical properties of hot-rolled and cold-formed steels. *J. Constr. Steel Res.* **2016**, *121*, 291–310. [[CrossRef](#)]
31. Mazzoni, S.; McKenna, F.; Scott, M.H.; Fenves, G.L. *OpenSees Command Language Manual*; Pacific Earthquake Engineering Research (PEER) Center: Berkeley, CA, USA, 2006; Volume 264, pp. 137–158.
32. Mehdizadeh, K.; Karamodin, A. Probabilistic assessment of steel moment frames incremental collapse (ordinary, intermediate and special) under earthquake. *J. Str. Constr. Eng.* **2017**, *4*, 129–147.
33. Ebrahimi Majumerd, M.J.; Mohammadi Dehcheshmeh, E.; Broujerdian, V.; Moradi, S. Self-centering rocking dual-core braced frames with buckling-restrained fuses. *J. Constr. Steel Res.* **2022**, *194*, 107322. [[CrossRef](#)]
34. Broujerdian, V.; Mohammadi Dehcheshmeh, E. Locating the rocking section in self-centering bi-rocking walls to achieve the best seismic performance. *Bull. Eq. Eng.* **2022**, *20*, 2441–2468. [[CrossRef](#)]
35. Mohammadi Dehcheshmeh, E.; Broujerdian, V. Determination of optimal behavior of self-centering multiple-rocking walls subjected to far-field and near-field ground motions. *J. Build. Eng.* **2022**, *45*, 103509. [[CrossRef](#)]

36. Suita, K.; Yamada, S.; Tada, M.; Kasai, K.; Matsuoka, Y.; Shimada, Y. Collapse experiment on 4-story steel moment frame: Part 2 detail of collapse behavior. In Proceedings of the 14th World Conference on Earthquake Engineering, Beijing, China, 12–17 October 2008.
37. Ramhormozian, S.; Charles Clifton, G.; Latour, M.; MacRae, G.A. Proposed simplified approach for the seismic analysis of multi-storey moment resisting framed buildings incorporating friction sliders. *Buildings* **2019**, *9*, 130. [[CrossRef](#)]
38. Department of Homeland Security. *Multi-Hazard Loss Estimation Methodology: Earthquake Model*; Federal Emergency Management Agency (FEMA): Washington, DC, USA, 2003; pp. 235–260.
39. Baker, J.W. Efficient analytical fragility function fitting using dynamic structural analysis. *Earthq. Spectra* **2015**, *31*, 579–599. [[CrossRef](#)]
40. Mohammadi Dehcheshmeh, E.; Broujerdian, V. Probabilistic Evaluation of Self-Centering Birocking Walls Subjected to Far-Field and Near-Field Ground Motions. *J. Str. Eng.* **2022**, *148*, 04022134. [[CrossRef](#)]

Disclaimer/Publisher's Note: The statements, opinions and data contained in all publications are solely those of the individual author(s) and contributor(s) and not of MDPI and/or the editor(s). MDPI and/or the editor(s) disclaim responsibility for any injury to people or property resulting from any ideas, methods, instructions or products referred to in the content.